J. Rosenzweig
Centre for Computational Science,
Queen Mary & Westfield College,
Mile End Road, London E1 4NS, UK
e-mail: J.Rosenzweig@qmul.ac.uk

O. E. Jensen
Division of Applied Mathematics,
School of Mathematical Sciences,
University of Nottingham, University Park,
Nottingham NG7 2RD, UK
e-mail: Oliver.Jensen@nottingham.ac.uk

Capillary-elastic Instabilities of Liquid-lined Lung Airways

To model the competition between capillary and elastic forces in controlling the shape of a small lung airway and its interior liquid lining, we compute the equilibrium configurations of a liquid-lined, externally pressurized, buckled elastic tube. We impose axial uniformity and assume that the liquid wets the tube wall with zero contact angle. Non-zero surface tension has a profound effect on the tube's quasi-steady inflation-deflation characteristics. At low liquid volumes, hysteresis arises through two distinct mechanisms, depending on the buckling wavenumber. Sufficient compression always leads to abrupt and irreversible collapse and flooding of the tube; flooding is promoted by increasing liquid volumes or surface tension. The model captures mechanisms whereby capillary-elastic instabilities can lead to airway closure. [DOI: 10.1115/1.1516811]

1 Introduction

When subject to external compression, small airways of the lung can undergo a buckling instability, whereby the epithelium and supporting basement membrane become folded, with the ridges of the folds running parallel to the axis of the airway. Lambert [1] identified the potential importance of the folded membrane as a load-bearing structure, and mechanical and geometric interactions between the folded membrane and the tissues surrounding it (submucosa and smooth muscle) have been extensively studied since then [2–5]. The folded membrane also interacts with the layer of liquid that coats the interior of each airway. The liquid lining is known to form pools in the interstices of a buckled airway wall [6]. The high curvature of the air-liquid interface in a pool leads to low capillary pressure in the liquid, which exerts a localized compressive stress on the airway wall. Capillary pressures can then compete with bending stresses in the folded membrane in determining the configuration of both the membrane and the liquid lining, surface tension trying to minimize the surface area of the liquid lining, and bending forces trying to minimize deformations of the airway wall.

This competition can have a number of important consequences. If surface tension is abnormally high (as is the case for premature infants suffering respiratory distress due to surfactant insufficiency) or if airway walls are abnormally deformable (as in emphysema), then capillary forces may overcome bending forces, leading to airway collapse. With an abnormally high volume of lining fluid (as in pulmonary edema), or when liquids are instilled into the lungs (as in partial liquid ventilation), collapse is likely to be accompanied by airway flooding, resulting in airway occlusion and (potentially) impaired gas exchange. When capillary and bending forces are of comparable magnitude, then abrupt changes in wall shape and liquid-lining distribution can be expected to occur during quasi-steady inflation and deflation of an individual airway [7], which may contribute in part to hysteresis in the overall pressure-volume characteristics of the whole lung. It is naturally desirable to understand the conditions leading to occlusion or hysteresis in individual airways.

The competition between capillary and elastic forces in an airway has been explored previously through a number of independent studies. Capillary instabilities of the liquid lining of a tube (analogous to the Rayleigh instability that causes a liquid jet to break up into drops) are well known to lead to liquid bridge formation in rigid cylindrical tubes [8,9], provided a sufficient volume of lining fluid is available, a process referred to as ''film collapse'' [10]. Using a model that assumed axisymmetry but allowed for axial nonuniformity, Halpern & Grotberg [11,12] showed how airway wall deformability promotes the formation of liquid bridges by reducing the critical fluid volume necessary for the tube to be occluded. They also showed how an axisymmetric elastic tube can collapse preferentially in an axially uniform mode, a process they called ''compliant collapse.'' However, no account was taken of the fact that an elastic tube buckles as it is compressed. To address this issue, Heil [13,14] used 3D finite element computations to compute the equilibrium configuration of an isolated liquid bridge in a non-axisymmetrically buckled elastic-walled tube, finding significant hysteresis in tube and liquid configurations as parameters are varied, accompanied by dramatic changes in bridge geometry. Using a simpler 2D model, Hill, Wilson and Lambert [7] modeled the airway wall as an axially uniform, thin-walled elastic tube, coated on its interior with a perfectly wetting fluid. They assumed that the wall buckles with azimuthal wavenumber $n=16$, and showed how the passage of a meniscus through a narrow gap between adjacent airway walls can lead to hysteresis in the quasi-steady pressure-area relation of the tube.

The aim of the present study is to extend the work of Hill et al. [7] to a significantly wider range of parameter space. In contrast to [7], we allow tubes to deform into configurations in which opposite walls come into contact, and we allow the tube to become flooded with lining liquid under sufficient external compression. By conducting an extensive survey of parameter space, we identify and classify possible pressure-area relations, which reveal some novel mechanisms of airway occlusion and collapse. Our study is also intended to complement Heil's computations (which were restricted to buckling of a tube to wavenumbers $n=2$ and $n=3$) within the framework of a substantially simpler mathematical model. We focus here on the buckling of a liquid-lined tube with wavenumbers $n=2$ (as illustrated in Fig. 1) and $n=4$. Supporting the choice $n=2$ are recent observations showing how airway closure in small airways of rabbits can occur initially by airway flattening, with little mucosal folding [15]. The effects of short airway lengths [14], parenchymal tethering [4,16] and airway wall inhomogeneities (both radial [5] and azimuthal [4]) can all contribute to mucosal buckling at higher wavenumbers. These effects can be modeled crudely by prescribing n, and rescaling wall parameters appropriately [7]. We take $n=4$ as representative of higher-order buckling. Our study also complements recent computations of Heil & White [17] who have examined the dynamic evolution of a liquid-lined elastic ring towards some of the static configurations we describe below.

Contributed by the Bioengineering Division for publication in the JOURNAL OF BIOMECHANICAL ENGINEERING. Manuscript received Mar. 2001; revised manuscript received Jul. 2002. Associate Editor: J. B. Grotberg.

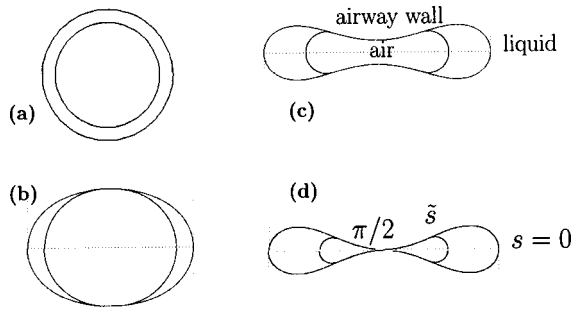

Fig. 1 The tube is initially circular and is lined with a film of uniform thickness; (*a*) As *p* is increased, the tube buckles (here into two lobes), and the film ruptures (*b*, *c*, *d*) to form a capillary meniscus, leaving part of the wall effectively dry. Opposite wall contact at $s=\pi/2$ is illustrated in (*d*).

2 The Model

Following [7], a small lung airway (of submillimeter diameter, so that gravitational forces are weak compared to capillary forces) is modeled as an inextensible, liquid-lined, axially uniform, thin-walled elastic tube of undeformed radius R and flexural rigidity $D=Eh^3/(1-\nu^2)$ (where E is Young's modulus, $h(\ll R)$ is wall thickness and ν is Poisson's ratio), loaded by the pressures applied to its inner and outer surfaces. The heterogeneous structure of the airway wall, and the effects of parenchymal tethering or smooth muscle constriction, are not accounted for explicitly in the present model. The difference between the external pressure (assumed uniform) and the air pressure within the tube is pD/R^3. The curvature of the wall $\kappa(s)/R$ varies with the arclength sR along the wall according to Euler–Bernoulli beam theory. In this approximation, the force balance in the wall can be reduced to a single differential equation for the dimensionless curvature κ [18,19]

$$\kappa_{ss}+\frac{1}{2}\kappa^3-c\kappa=\mathcal{P} \quad (0\leqslant s<2\pi), \tag{1}$$

where $\mathcal{P}(s)D/R^3$ is the negative transmural pressure and a subscript s denotes differentiation with respect to arclength. c is a constant (to be determined) that relates the outward normal force $DN(s)/R^2$ on the wall to the curvature via $N=c-\frac{\kappa^2}{2}$. Under external compression, the tube buckles to nonaxisymmetric configurations. We assume here that it buckles to shapes with n-fold symmetry (where $n\geqslant 2$), forming n identical lobes. It is then only necessary to compute the wall shape between two axes of symmetry, from a point of maximal curvature ($s=0$) to the nearest point of minimal curvature ($s=\pi/n$). Tube shapes and liquid-lining distributions in the case $n=2$ are illustrated in Fig. 1.

Denoting the air-liquid surface tension as $\sigma^*=\sigma D/R^2$ and the radius of curvature of the air-liquid interface as aR, the dimensionless pressure drop across the wall $\mathcal{P}$ has the form

$$\mathcal{P}=p+(\sigma/a) \tag{2}$$

when the film is continuous (as in Fig. 1(*a*)), and

$$\mathcal{P}(s;\tilde{s})=\begin{cases} p+\sigma/a & \text{if } 0<s<\tilde{s} \\ p+\sigma\kappa(s) & \text{if } \tilde{s}<s<\pi/n \end{cases} \tag{3}$$

after film rupture, when the meniscus meets the wall at a contact line $s=\tilde{s}$, as shown in Fig. 1(*b–d*). We assume that the fluid is perfectly wetting so that the meniscus meets the wall with zero contact angle at $s=\tilde{s}$. As in [7], we assume that the "dry" portion of the wall is covered with a film of zero thickness but non-zero surface tension, an assumption which is consistent with continuity of wall tension across the contact line.

The variables a and $\tilde{s}$ are determined from the requirement that the fluid volume per unit length should be conserved and equal to a prescribed value V_lR^2. The volume constraint is

$$V_l=V-a^2\pi, \quad \text{where } V=\frac{1}{2}\int_0^{2\pi}\mathbf{x}.\mathbf{n}\,ds \tag{4}$$

when the air-fluid interface is continuous, and

$$\frac{V_l}{2n}=\frac{1}{2}\int_0^{\tilde{s}}\mathbf{x}.\mathbf{n}\,ds+\frac{a^2}{2}(\sin\varphi(\tilde{s})\cos\varphi(\tilde{s})-\varphi(\tilde{s})) \tag{5}$$

when the air-fluid interface is ruptured. V, the tube's volume per unit length, is used as a measure of the deformation of the tube. Here

$$\mathbf{x}(s)=(x(s),y(s))=\int_0^s(\cos\varphi(\zeta),\sin\varphi(\zeta))d\zeta \tag{6}$$

represents a point on the wall, the tangent angle $\varphi(s)$ is defined by

$$\varphi(s)=\int_0^s\kappa(\xi)d\xi, \tag{7}$$

and the outward unit normal to the wall is $\mathbf{n}(s)=(\sin\varphi(s), -\cos\varphi(s))$. The zero-contact-angle condition at $s=\tilde{s}$ is

$$x(\tilde{s})=a\sin\varphi(\tilde{s}). \tag{8}$$

Boundary and integral conditions on Eq. (1) for a buckled tube with n lobes are

$$\kappa_s(0)=\kappa_s(\pi/n)=0, \quad \int_0^{\pi/n}\kappa\,ds=\pi/n \tag{9}$$

when the opposite walls are not in contact (Fig. 1(*a–c*)), and are modified as described by [18] when the opposite walls are in contact (Fig. 1(*d*)). For buckling in two lobes, opposite wall contact (OWC) occurs at the point $s=\pi/2$; in this case we replace $\kappa_s(\pi/2)=0$ in Eq. (9) with $\kappa(\pi/2)=-\sqrt{2c}$ (implying zero normal force on the wall). For $n>2$, contact occurs at a point s_0 to be determined, in which case Eq. (9) is supplemented with

$$\kappa(s_0)=-\sqrt{2c}, \quad \int_0^{s_0}\kappa ds=\frac{\pi}{2}.$$

We discretized Eqs. (1–3) with appropriate integral and boundary conditions using uniformly spaced finite differences, and solved the resulting algebraic system with Newton's method for a given approximation to $\tilde{s}$ and a. This approximation was then corrected using Powell's hybrid method (from the NAG library) to minimize the errors in the constraints Eqs. (4–8). The process was repeated until convergence. A continuation method was employed, starting from the axisymmetric state and decreasing V in fixed increments, checking the topology at each step, to yield the relationship between p and V for fixed V_l, σ and n. The code was run with meshes of 500, 1000 and 2000 grid points per half-lobe; the resulting $p-V$ curves exhibited negligible dependence on mesh size.

3 Results

We present first a perturbation analysis of the effect of the fluid film on the primary buckling instability, and then describe the numerical solution to the fully nonlinear problem for the cases $n=2$ and $n=4$.

3.1 Primary Buckling Bifurcation. A weakly nonlinear asymptotic analysis (Appendix A) shows that the tube remains circular for low values of p, but that it buckles in n lobes when p exceeds

$$p_{buc}^{(n)}=n^2-1-\sigma(1-(V_l/\pi))^{-1/2}. \tag{10}$$

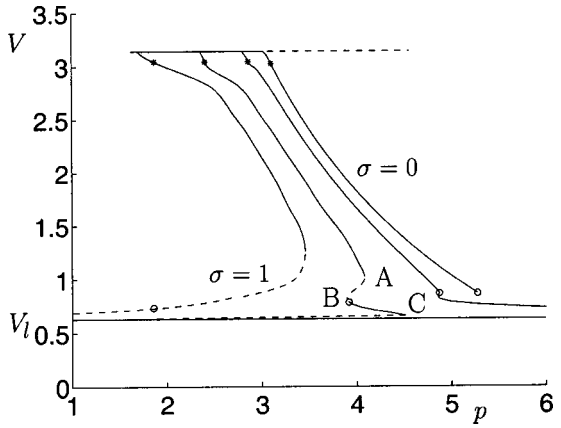

Fig. 2 Pressure-volume curves for $n=2$, $V_l=\pi/5$ and $\sigma=0$, 0.4, 0.6, 1. Film rupture is denoted by * and opposite wall contact by ○. Stable (unstable) solution branches are shown solid (dotted).

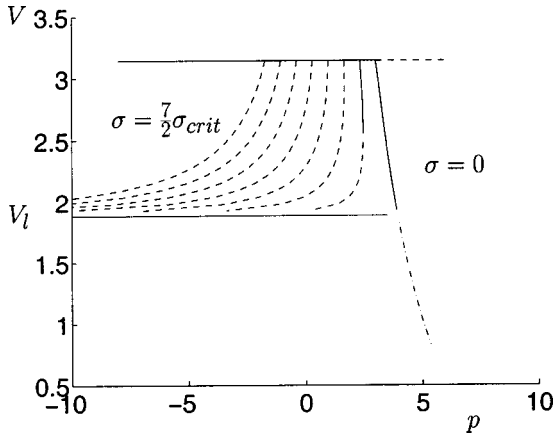

Fig. 3 Pressure-volume curves for $n=2$, $V_l=3\pi/5$ and $\sigma/\sigma_{crit}=0$, 1/2, 1,. . . 7/2. Stable (unstable) solution branches are shown solid (dashed). The dash-dotted line shows the $p-V$ curve for $\sigma=0$, $V_{fl}=0$.

Thus the most unstable mode is $n=2$ (in this simple model), and for any fixed n increasing surface tension or fluid volume reduces the load required for the tube to buckle, but does not change the preferred wavenumber. Further, the buckling bifurcation is supercritical for $\sigma<\sigma_{crit}$, where

$$\sigma_{crit}=\frac{3}{2}(n^2-1)^2 n^{-2}(1-(V_l/\pi))^{3/2} \tag{11}$$

(implying that increasing the load p leads to a reduction in tube volume V), but it becomes subcritical for $\sigma>\sigma_{crit}$. With p as a control parameter, this implies that the buckled solutions are stable for $\sigma<\sigma_{crit}$, but unstable otherwise. These predictions, which hold only in the vicinity of the buckling point, will be illustrated below using solutions of the fully nonlinear problem.

3.2 Two Lobes of Buckling. Numerically computed $p-V$ curves for $n=2$ and $V_l=\pi/5$ are shown in Fig. 2. The solution for $\sigma=0$ shows the usual monotonic post-buckling deformation [18], where an increase in external pressure causes a decrease in tube volume. The liquid lining ruptures shortly after the tube buckles. Increasing σ (say to 0.6 on Fig. 2) introduces three major changes to the $p-V$ curve. First, the buckling pressure is reduced, as predicted by Eq. (10). Second, a region of hysteresis arises (between folds A and B in the curve). The solution branch between the two folds, for which $dV/dp>0$, is unstable if p is taken as a control parameter, so that the tube will jump abruptly between stable solution branches as p is varied. Opposite wall contact (OWC) occurs close to fold B, and this restabilizes the lower solution branch; the stabilizing effects of OWC were also noted in [13,14]. Third, as V falls towards V_l, the meniscus is pushed towards the point of OWC. In doing so, the curvature of the meniscus falls rapidly, as does the pressure in the liquid (relative to that in the air), which is strongly destabilizing. This induces a third fold (C) in the pressure-volume curve, and leads to an unstable solution branch which asymptotes to the completely flooded state $V=V_l$, with $p\propto-(V-V_l)^{-2/3}$ as $V\to V_l$ (Appendix B). A further increase in σ (*e.g.* to $\sigma=1$ on Fig. 2) increases the destabilizing effect of surface tension: the buckling pressure is reduced further still, the stabilizing effects of OWC are eliminated, and the stable solution branch BC is lost. In this case, increasing p beyond about 3.5 leads to abrupt collapse and flooding. There is no means of reopening a flooded tube within this simple 2D model.

Reversible hysteresis, such as that near $p=4$ for $\sigma=0.6$ in Fig. 2, involving the two adjacent folds A and B in the $p-V$ curve, arises because OWC restabilizes the lower solution branch. It can only therefore occur if V_l is sufficiently low that the tube does not flood before OWC. An empty tube first experiences OWC at a volume $\tilde{V}_1\approx 0.2694\pi$ [18]. A necessary condition for this class of hysteresis is therefore $V_l<\tilde{V}_1$.

Typical solutions for $V_l>\tilde{V}_1$ are shown in Fig. 3. As expected, no reversible hysteresis is found. Again, increasing σ reduces the pressure at which the primary buckling bifurcation occurs. The bifurcation changes from supercritical to subcritical as σ passes through σ_{crit} (see Eq. (11)). This corresponds to the movement of the fold seen for $\sigma=\sigma_{crit}/2$ in Fig. 3 towards the uniform solution branch $V=\pi$. For all $\sigma>0$ with $V_l>\tilde{V}_1$, the tube floods abruptly and irreversibly if p is increased sufficiently, either from a collapsed state (if $\sigma<\sigma_{crit}$) or from the fully open state (for $\sigma>\sigma_{crit}$). Flooding occurs before opposite walls can come into contact, so that just before flooding, the liquid lining becomes continuous around the tube, trapping a small bubble of air. The high curvature of the bubble creates a low and highly destabilizing capillary pressure in the tube, making this instability a nonaxisymmetric form of the compliant collapse seen in [11]. For $V\to V_l$, the bubble radius $a=[(V-V_l)/\pi]^{1/2}\to 0$, the transmural pressure $\mathcal{P}\to p_0(V_l)$ (where $p_0(V)=O(1)$ is the monotonic pressure-volume relation for a dry tube), and Eq. (2) implies $p\approx p_0(V_l)-\sigma/a$. The capillary term $-\sigma/a$ dominates the elastic term, and the (unstable) solution branch asymptotes to the flooded state $V=V_l$ with

$$p\approx-\sigma\sqrt{\pi}(V-V_l)^{-1/2} \quad \text{as} \quad V\to V_l. \tag{12}$$

We conducted a survey of (σ,V_l)-parameter space for two-lobed buckled states, from which we have constructed the map shown in Fig. 4. It consists of five distinct regions. Computing some of the boundaries between regions was expensive, so we indicate their approximate location by connecting individual computed points with straight lines. For low σ and low V, $p-V$ curves are monotonic until the tube is close to flooding (region (i)). For $\sigma>0$, the tube always floods irreversibly if p is increased sufficiently. Increasing σ, at low liquid volumes, introduces reversible hysteresis in the inflation-deflation cycle, where OWC is required to restabilize the lower stable solution branch (region (ii)). Further increase in σ makes the primary buckling bifurcation subcritical, so that as p is increased an initially uniform tube will jump abruptly either to a collapsed, open state or a completely flooded state (region (iii)). Increasing V_l eliminates the region of reversible hysteresis, and reduces the external load required to cause irreversible flooding, which occurs either from a collapsed state (region (iv)) or from the fully open state (region (v)). Transitions between regions (i), (ii) and (iv) are depicted in Fig. 2, and that from (iv) to (v) is shown in Fig. 3.

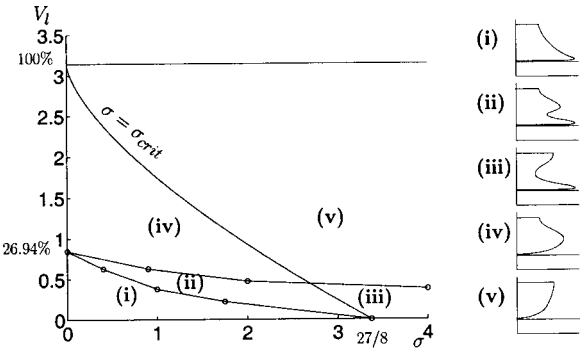

Fig. 4 (σ, V_l) parameter space, $n=2$. Insets show typical $p-V$ curves for regions (i)–(v) of parameter space. Circles denote computed points, accurate to $V_l \pm 0.01$; they are connected by straight lines.

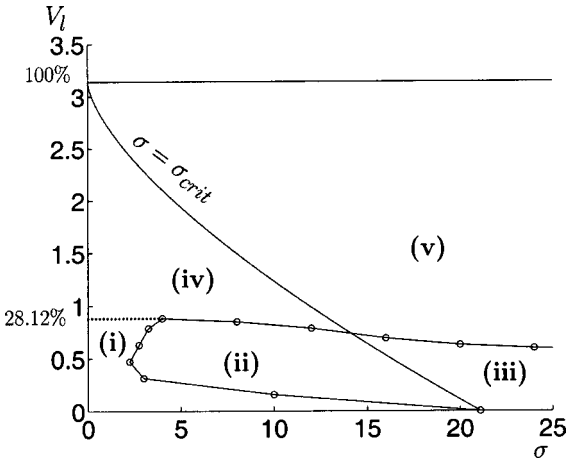

Fig. 6 (σ, V_l) parameter space, $n=4$. The typical $p-V$ curves for regions (i)–(v) are as illustrated in Fig. 4. Circles denote computed points, accurate to $V_l \pm 0.01$; they are connected by straight lines.

3.3 Several Lobes of Buckling. The primary difference between the cases $n=2$ and $n>2$ is that, in the former case, the neck of the lobe (the narrowest point of the cross-section) coincides with the point of symmetry π/n, whereas for $n>2$ it does not. This subtle difference in geometry causes a significant difference in the mechanism for folding of $p-V$ curves at high σ, as illustrated in Fig. 5 for $n=4$, $V_l=3\pi/20$.

For $\sigma=0$, the film ruptures shortly after the tube buckles. The meniscus passes through the neck of the lobe (as illustrated in the insets to Fig. 5), and then the film becomes continuous again as V approaches V_l, with air trapped as a shrinking bubble in the tube. For $\sigma>0$, the tube therefore experiences compliant collapse: the analysis leading to Eq. (12) applies once the bubble has formed, and all solution curves exhibit a fold shortly after the air-liquid interface detaches from the wall, with an unstable solution branch asymptoting to the flooded branch $V=V_l$. As σ increases (e.g., $\sigma=3$ in Fig. 5), a region of reversible hysteresis also arises (between folds A and B). This is analogous to that noted in [7] for the case $n=16$. As the meniscus passes through the neck of the lobe, its curvature rises, which lowers the capillary pressure; this is a destabilizing effect, leading to fold A. As V falls, the meniscus passes out of the neck, its curvature falls again and the solution branch restabilizes at fold B.

A necessary condition for fold B to exist is that the meniscus passes through the neck before the air-liquid interface detaches from the wall. We define V_c as the volume within a dry tube at the first point of OWC minus the volume of the largest spherical cylinder that can be inscribed in the central portion of the tube. For $n=4$, $V_c \approx 0.2812 \times \pi$; this provides an approximate bound on values of V_l above which the fold cannot exist. For $V_l > V_c$, we found that solution curves resembled those shown in Fig. 3: there is no mechanism for reversible hysteresis, and instead as p increases there is abrupt flooding of the tube from large volumes, either from collapsed states ($\sigma < \sigma_{crit}$) or from the circular state ($\sigma > \sigma_{crit}$), via compliant collapse.

A map of (σ, V_l)-parameter space for $n=4$, analogous to that for $n=2$, is shown in Fig. 6. Again, five regions are identified. When σ and V_l are sufficiently low (region (i)) the tube buckles supercritically, and it eventually experiences abrupt flooding via compliant collapse. As σ is increased (keeping $V_l < V_c$, region (ii)) the primary buckling bifurcation remains supercritical, but reversible hysteresis can occur in addition to abrupt flooding via compliant collapse. The transition between regions (i) and (ii) is illustrated in Fig. 5. As σ is increased beyond σ_{crit} (region (iii)), the buckling bifurcation becomes subcritical and the $p-V$ curve has just two folds: in this case abrupt flooding may occur either from a collapsed state or from the circular state. (For low V_l, the neck closes in OWC while the air-fluid interface and the contact line are still inside the lobe. In this case we assumed that the contact line can move freely through the closed neck. While it was not possible to compute $p-V$ curves within a small neighborhood of the point at which the contact line passed through the point of OWC, we found no indication that OWC had any qualitative effects on the $p-V$ curve for $n>2$.) For sufficiently large V_l, reversible hysteresis is suppressed by compliant collapse and we recover regions (iv) and (v), much as for $n=2$. The condition $V_l > V_c$ provides a robust condition ensuring the absence of reversible hysteresis; it separates regions (i) and (iv), although they are essentially equivalent. Computations were carried out for a range of wavenumbers n and the behavior described above appears to be generic for $n>2$, although we cannot rule out the possibility that the two independent mechanisms of hysteresis exhibited by this model for $n=2$ and $n=4$ may not both arise in some part of parameter space.

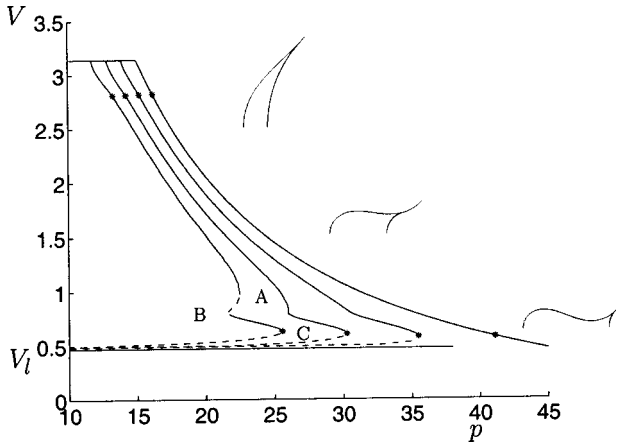

Fig. 5 Pressure-volume curves for $n=4$, $V_l/\pi=0.15$ and $\sigma=0, 1, 2, 3$, with σ increasing from right to left. Film rupture and reattachment are labeled by *. Stable (unstable) solution branches are shown solid (dashed). The centerlines of the pictures of half-lobes at various degrees of collapse correspond to their respective values of V.

4 Discussion

Despite the neglect of numerous effects, we believe the simple model presented here captures some significant features of the quasi-static inflation-deflation characteristics of a liquid-lined lung airway. The governing parameters of the model are n (the buck-

ling wavenumber), $\sigma=\sigma^* R^2/D$ (measuring the ratio of surface tension σ^* to membrane flexural rigidity D) and V_l (the proportion of the tube lumen occupied by fluid). Maps of (σ, V_l)-parameter space show broadly similar behavior for both $n=2$ (Fig. 4) and $n>2$ (Fig. 6). For $\sigma>0$, the model predicts that sufficient compression of the tube always leads to abrupt collapse and flooding. Flooding occurs in two ways: at low V_l, the meniscus is squeezed into a narrow gap between touching membranes (Appendix B); at high V_l, the air-liquid interface detaches from the membrane forming a bubble within the tube. In each case, as the tube is compressed, elastic forces are too weak to counter increasingly low capillary pressures, leading to instability. The load required to flood the tube reduces as σ and V_l increase, so much so that for σ and V_l sufficiently large, the primary buckling bifurcation is subcritical (Eq. (11)), and a circular tube buckles immediately to a fully flooded state (region (v), Figs. 4, 6). Two distinct mechanisms of reversible hysteresis are also identified at low V_l and large σ (regions (ii) and (iii), Figs. 4, 6), one stabilized by opposite wall contact (for $n=2$, Fig. 2), and one involving passage of a meniscus through the neck of a lobe (requiring $n>2$, Fig. 5). The former captures qualitative behavior seen in 3D models [13,14], while the latter was observed previously in [7]. Even when σ is small, sufficiently large fluid volumes promote abrupt flooding at modest external loads (region (iv), Figs. 4, 6). Similarly, at low fluid volumes, with the tube almost dry, sufficiently high σ ($\sigma>3(n^2-1)^2/(2n^2)$) leads to snap-through from the uniform state at low loads (region (iii), contrary to claims in [7] that small V_l has little effect).

The results presented here are broadly consistent with recent computations of the unsteady version of this problem (using Lagrangian shell theory and the Navier–Stokes equations) by Heil and White [17]. For fixed V_l and $n=2$, they show simulations for increasing values of σ that demonstrate the transition between type-(iv) and type-(v) behavior (Fig. 4). However for their choice of wall thickness ($h=R/20$), our prediction of the boundary between these two regions (σ_{crit}) is qualitatively but not quantitatively accurate. This is likely to be because σ has a strongly nonlinear dependence on wall thickness ($\sigma\propto h^{-3}$), suggesting that finite-thickness effects have a substantial effect on the location of stability boundaries in parameter space.

This simple physical model of a lung airway can be interpreted in two ways. First, for buckling with wavenumber $n=2$, we may suppose that the membrane represents the entire thickness of the airway wall, and then the model mimics the flattening of airways seen recently in a rabbit model [15]. Alternatively, for $n>2$, the membrane models folding of the epithelium and its basement membrane (following [7]), with the effects of tethering in the submucosa [4] or geometric constraints due to smooth muscle [3] lumped into the parameters n, p and σ. As the computations in [17] suggest, σ is sensitive to wall structure and thickness. Values of σ used in the literature range between 6 [14] and 100–200 [7,11,17]: larger values are appropriate when considering mucosal buckling at high wavenumbers. For a 1 mm radius airway, which flattens with $n=2$ at a buckling pressure of roughly 2 cm H_2O [15], $\sigma\approx 0.1$ when $\sigma^*\approx 20$ dyn/cm: while this is not large enough for capillary-elastic instabilities to be expected immediately, factors such as increased surface tension due to surfactant inactivation, reduced wall thickness (perhaps due to smooth muscle relaxation), reduced Young's modulus, or increased liquid volume (in edema, or if liquids are instilled in the airways) could readily increase σ to values at which capillary effects become significant. In contrast, the recent estimate $D\approx 10^{-12}$ Pa·m^3 for the flexural rigidity of folded epithelium of peripheral rabbit airways [20] (for which $\sigma\approx 10^4$ in a 1 mm airway with $\sigma^*=10$ dyn/cm) suggests that significant capillary-elastic interactions can be anticipated even under normal conditions.

In our analysis both the fluid and solid motions have been assumed to be quasi-steady, following a scaling argument [7] showing that draining flows are very rapid on the time scale of breathing for small airways (with $R\leqslant 1$ mm). Studies of model draining flows on surfaces of non-uniform curvature reveal an intricate asymptotic structure at large times, which may well be influenced by wall stretching due to breathing [21]. Naturally, the abrupt transitions predicted here will themselves occur on fast timescales, over which viscous and inertial forces in both the liquid and the tube wall can be significant [17]. Dynamic effects may also lead to liquid lining distributions not considered in the present model: for example, snap-off from the uniform state with $n=2$ may lead to a liquid bridge trapped at the narrowest point of the tube. The present model does not account for this possibility, and so cannot capture a potential further mechanism of hysteresis as such bridges are formed and broken during airway volume cycling. Most significantly, this study neglects many important effects associated with the tube's third dimension, associated with capillary instabilities [11,12], mechanisms of airway reopening [22,23] and occlusion by liquid bridges [13,14], and this deficiency should be addressed in future studies.

In summary, this study identifies regions in governing parameter space in which an axially uniform, liquid-lined tube experiences reversible hysteresis during its inflation-deflation cycle, abrupt and irreversible flooding under sufficient compression, or both. Liquid volume (per unit length) in excess of a critical value (about 30% for $n=2$ and $n=4$) eliminates hysteresis but promotes abrupt flooding. Even at smaller volumes, sufficiently high surface tension can lead to snap-through and flooding. While a healthy airway maintains low fluid volumes and low surface tension, this study shows how a variety of pathologies may make the airway susceptible to capillary-elastic instabilities that induce airway collapse and occlusion.

Appendix A

When the tube is close to the undeformed state ($\kappa\approx 1$), the air-liquid interface is circular with radius a and the transmural pressure is uniform and given by Eq. (2). By regular perturbation about the undeformed state [19], with error $O(\varepsilon^3)$, we find that

$$\kappa(s)=1+\varepsilon\cos ns+\frac{1}{4}\varepsilon^2 n^{-2}(\cos 2ns-\cos ns),$$

$$c=\left(\frac{3}{2}-n^2\right)+3\varepsilon^2 n^{-2}(n^2+1)/8,$$

$$\mathcal{P}=(n^2-1)+3\varepsilon^2 n^{-2}(n^2-1)/8$$

for some disturbance amplitude $\varepsilon\ll 1$. Thus $V=\pi-\varepsilon^2\pi/[2(n^2-1)]$, and so Eq. (4) implies $a=a_0-\varepsilon^2/[4(n^2-1)a_0]$, where $a_0=(1-V_l/\pi)^{1/2}$. Then Eq. (2) gives

$$p=p_{buc}^{(n)}+\frac{3\varepsilon^2}{8}\left(\frac{n^2-1}{n^2}-\frac{2\sigma}{3(n^2-1)a_0^3}\right), \tag{13}$$

where $p_{buc}^{(n)}$ is given by Eq. (10). The buckling bifurcation is supercritical if the bracketed term in Eq. (13) is positive, leading to Eq. (11).

Appendix B

Consider the case $n=2$ with the tube in OWC at $s=\pi/2$. Here $\kappa(\pi/2)=-\sqrt{2c}=-1/R$, say, for some $R>0$, $c>0$, where $R=O(1)$. Locally, the tube is parabolic with shape $y=\pm x^2/(2R)$. Suppose the meniscus lies very close to the corner, with the contact line at $x=\xi R$, where $\xi\ll 1$. Then to leading order in ξ, the volume of air is $V_g\approx 2R^2\xi^3/3$, the radius of curvature of the meniscus is $a\approx R\xi^2/2$, so the liquid pressure is $p=-2\sigma/(R\xi^2)$. There is a large jump in transmural pressure over a short distance; the wall curvature however varies over an $O(1)$ lengthscale (from Eq. (1)), and so is uniform to leading order in the neighborhood of the contact line.

Now consider the family of solutions computed in [18] for a dry tube with opposite walls in point contact, with volume $\tilde{V}(\tilde{p})$ and curvature at the contact point $\tilde{R}(\tilde{p})$, where the negative transmural pressure $\tilde{p}$ varies between approximately 5.247 (the first point of OWC, where $\tilde{V}=\tilde{V}_1\approx 0.846$) and 10.34 (where $\tilde{V}=\tilde{V}_2<\tilde{V}_1$, and the solution changes from point to line contact). For $\tilde{V}_2<V_l<\tilde{V}_1$, there is a unique $\tilde{p}_l$ for which $\tilde{V}(\tilde{p}_l)=V_l$, and a corresponding $\tilde{R}_l=\tilde{R}(\tilde{p}_l)$.

For a wet tube, when the air-liquid interface is very close to the contact point,

$$V\approx\tilde{V}(\tilde{p})\approx V_l+2R^2\xi^3/3,\quad \tilde{p}\approx p+2\sigma/(R\xi^2), \tag{14}$$

where $R\approx\tilde{R}(\tilde{p})$. Then as $V\to V_l$, Eq. (14) implies

$$p\approx\tilde{p}_l-2^{5/3}\sigma\tilde{R}_l^{1/3}[3(V-V_l)]^{-2/3},$$

implying the solution branch asymptotes to $p\to-\infty$ as $V\to V_l$. For $V_l<\tilde{V}_2$, a similar argument indicates flooding occurs after line, rather than point, contact.

Acknowledgments

JR is grateful to Gonville & Caius College, University of Cambridge, for support from an Elmore Studentship.

References

[1] Lambert, R. K., 1991, ''Role of Bronchial Basement Membrane in Airway Collapse,'' J. Appl. Physiol., **81**, pp. 666–673.
[2] Kamm, R. D., 1999, ''Airway Wall Mechanics,'' Annual Review of Biomedical Engineering, **1**, pp. 47–72.
[3] Lambert, R. K., Codd, S. L., Alley, M. R., and Pack, R. J., 1994, ''Physical Determinants of Bronchial Mucosal Folding,'' J. Appl. Physiol., **77**, pp. 1206–1216.
[4] Seo, C. Y., Wang, L., and Paré, P. D., 2000, ''Airway Narrowing and Internal Structural Constraints,'' J. Appl. Physiol., **88**, pp. 527–533.
[5] Wiggs, B. R., Hrousis, C. A., Drazen, J. M., and Kamm, R. D., 1997, ''On the Mechanism of Mucosal Folding in Normal and Asthmatic Airways,'' J. Appl. Physiol., **83**, pp. 1814–1821.
[6] Yager, D., Butler, J. P., Bastacky, J., Israel, E., Smith, G., and Drazen, J. M., 1989, ''Amplification of Airway Constriction due to Liquid Filling of Airway Interstices,'' J. Appl. Physiol., **66**, pp. 2873–2884.
[7] Hill, M. J., Wilson, T. E., and Lambert, R. K., 1997, ''Effects of Surface Tension and Intraluminal Fluid on Mechanics of Small Airways,'' J. Appl. Physiol., **18**, pp. 233–239.
[8] Grotberg, J. B., 1994, ''Pulmonary Flow and Transport Phenomena,'' Annu. Rev. Fluid Mech., **26**, pp. 529–571.
[9] Johnson, M., Kamm, R. D., Ho, L. W., Shapiro, A., and Pedley, T. J., 1991, ''The Nonlinear Growth of Surface-tension-driven Instabilities of a Thin Annular Film,'' J. Fluid Mech., **233**, pp. 141–156.
[10] Kamm, R. D., and Schroter, R. C., 1983, ''Is Airway Closure caused by a Liquid Film Instability?'' Respir. Physiol., **75**, pp. 141–156.
[11] Halpern, D., and Grotberg, J. B., 1992, ''Fluid-elastic Instabilities of Liquid-lined Flexible Tubes,'' J. Fluid Mech., **244**, pp. 615–632.
[12] Halpern, D., and Grotberg, J. B., 1993, ''Surfactant Effects on Fluid-elastic Instabilities of Liquid-lined Flexible Tubes: a Model of Airway Closure'' ASME J. Biomech. Eng., **119**, pp. 271–277.
[13] Heil, M., 1998, ''Minimal Liquid Bridges in Non-axisymmetrically Buckled Elastic Tubes,'' J. Fluid Mech., **380**, pp. 309–337.
[14] Heil, M., 1999, ''Airway Closure: Occluding Liquid Bridges in Strongly Buckled Elastic Tubes,'' ASME J. Biomech. Eng., **121**, pp. 487–493.
[15] Okazawa, M., Paré, P. D., and Lambert, R. K., 2000, ''Compliance of Peripheral Airways Deduced from Morphometry,'' J. Appl. Physiol., **89**, pp. 2373–2381.
[16] Wang, C. Y., Watson, L. T., and Kamat, M. P., 1983, ''Buckling, Postbuckling, and the Flow through a Tethered Elastic Cylinder under External Pressure,'' J. Appl. Mech., **50**, pp. 13–18.
[17] Heil, M., and White, J. P., 2002, ''Airway Closure: Surface-tension-driven Non-axisymmetric Instabilities of Liquid-lined Elastic Rings,'' J. Fluid Mech., **462**, pp. 79–109.
[18] Flaherty, J. E., Keller, J. B., and Rubinow, S. I., 1972, ''Post-buckling Behavior of Elastic Tubes and Rings with Opposite Sides in Contact,'' SIAM (Soc. Ind. Appl. Math.) J. Appl. Math., **23**, pp. 446–455.
[19] Tadjbakhsh, I., and Odeh, F., 1967, ''Equilibrium States of Elastic Rings,'' J. Math. Anal. Appl., **18**, pp. 59–74.
[20] Lambert, R. K., Paré, P. D., and Okazawa, M., 2001, ''Stiffness of Peripheral Airway Folding Membrane in Rabbits,'' J. Appl. Physiol., **90**, pp. 2041–2047.
[21] Rosenzweig, J., 2000, ''Capillary-elastic Instabilities and Draining Flows in Buckled Lung Airways,'' Ph.D. thesis, University of Cambridge.
[22] Gaver, D. P. III, Halpern, D., Jensen, O. E., and Grotberg, J. B., 1996, ''The Steady Motion of a Semi-infinite Bubble through a Flexible-walled Channel,'' J. Fluid Mech., **319**, pp. 25–65.
[23] Jensen, O. E., Horsburgh, M. K., Halpern, D., and Gaver, D. P. III, 2002, ''The Steady Propagation of a Bubble in a Flexible-walled Channel: Asymptotic and Computational Models,'' Phys. Fluids, **14**, pp. 443–457.